ACS Biomaterials SCIENCE & ENGINEERING

pubs.acs.org/journal/abseba

Methods/Protocols

A Microfabrication Method of PCL Scaffolds for Tissue Engineering by Simultaneous Two PDMS Molds Replication

Hassan Najafi sani, Karen Abrinia, Nooshin Haghighipour, Daniel George, Yves Remond, and Majid Baniassadi*

Cite This: *ACS Biomater. Sci. Eng.* 2021, 7, 4763–4778

Read Online

ACCESS | Metrics & More | Article Recommendations

ABSTRACT: Not very far away, "tissue engineering" will become one of the most important branches of medical science for curing many types of diseases. This branch needs the cooperation of a wide range of sciences like medicine, chemistry, cellular biology, and genetic and mechanical engineering. Different parameters affect the final produced tissue, but the most important one is the quality and biocompatibility of the scaffold with the desired tissue which can provide the functionality of "native ECM" as well. The quality of the scaffold is directly dependent on its materials, design, and method of fabrication. As to the design and fabrication, there are two main categories: (a) random microporosity such as phase separation, electrospinning, and fused deposition modeling (3D printing) and (b) designed microporosity mostly achievable by stereo lithography and soft lithography. The method of fabrication implemented in this research is a novel method in soft lithography employing a type of "replica molding" with one pair of polydimethylsiloxane (PDMS) molds in contrast to traditional replica molding with just one single mold. In this operation, the solution of polycaprolactone in chloroform is initially prepared, and one droplet of the solution is placed between the molds while a preset pressure is applied to maintain the molds tightly together during the solidification of the polymer layer and vaporization of the solvent. Thus, a perfect warp and woof pattern is created. In this research, it has been approved that this is a feasible method for creating complex patterns and simple straight fiber patterns with different spacings and pore sizes. Cell attachment and migration was studied to find the optimum pore size. It was shown that the small pore size improves the cells' adhesion while reducing cell migration capability within the scaffold.

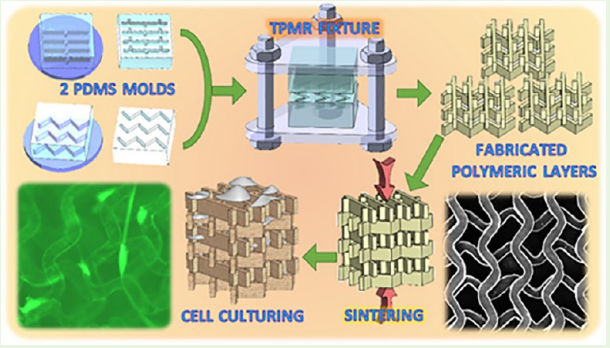

KEYWORDS: *Tissue engineering, Scaffold, Two PDMS molds, Replica molding, soft lithography, Cell culturing*

1. INTRODUCTION

Synthetic or natural scaffolds have a crucial role in tissue engineering dating back to the 1980s.[1] Different methods can be used for their fabrication, with the ideal objective of being most similar to the native extra cellular matrix (ECM) in topography, geometry, and micro- and nanostructure.[2] With native ECM consisting of nanofibers bringing integrity to the tissue, new fabrication methods like electrospinning (ES) and self-assembly can be used to make nanofiber structures and increase the area to volume ratio to improve cell attachment and migration.[3] Hutmacher[4] showed that in the calcium phosphate scaffold, the size of micropores is very important. It must be large enough for the cells, nutrients, and oxygen to penetrate the scaffold through adequate pore interconnectivity. Other works concentrated on silk polymers to fabricate the mentioned structure using phase separation[5] and solid–liquid separation.[6] Wnek and Bowlin[7] used particle leaching with different progen materials like sugar, salt, and gelatin, while Riley et al.[8] showed that if the progen size decreases, the depth of penetration will increase due to the increase of pores' interconnectivity.

In recent years, ES showed a good capability for creating a nanofiber pattern.[9] Matthews et al.[10] used this method to fabricate a collagen–elastin scaffold, but using biological materials as a base remains a challenge. A wide range of synthetic and natural polymers such as polydioxanone can nowadays be used in the ES technique.[11] Stankevich et al.[12] fabricated some PCL scaffolds by ES and modified them by reactive magnetron sputtering. ES can be used in wound dressing,[13] cartilage,[14] bone,[15] and nerve[16] tissue production. Baker et al. used a novel method assisted with atomic force

Received: May 15, 2021
Accepted: August 31, 2021
Published: September 13, 2021

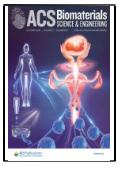

https://doi.org/10.1021/acsbiomaterials.1c00651
ACS Biomater. Sci. Eng. 2021, 7, 4763–4778

microscopy to exactly measure the strength of polycaprolactone nanofibers and obtain elastic behavior as well as a stress strain curve of this type of polymer.[17] In novel research, Brown et al.[18] used Direct Writing by Electrospinning (DWBE) fibers on a 2D moving collector. Using a rapid moving collector as the base plate, Brown succeeded in augmenting various layers which are basically very similar in nature to 3D printing. The high velocity of the collector caused the ejected molten fiber in a way to avoid tangling and at the same time be stretched thin enough. In this method, Brown used a molten flow of PCL for producing different diameter fibers including 6, 12.5, and 20 μm. The 20-μm fibers were used to fabricate structures similar to 3D printing by stacking various layers. However, one difficulty of this method is the control of appropriate porosity for the cultured cells, especially in random fiber deposition, to penetrate inside the scaffold, and the lack of similarity between microstructure distribution and the biological tissue. Thus, researchers have examined other methods based on computer-aided design to create specifically defined microstructure scaffolds. To achieve this goal, new devices and methods are necessary to create complex scaffolds and control the cells distribution and penetration, as well as their interactions with scaffold.[19] Falconnet[20] emphasized that the development in this area is not only limited to the creation of a more accurate architecture medium but also depends on the scaffold as an active component to lead the tissue development process. For example, rapid prototyping and 3D printing such as a streolithography apparatus (SLA) and fused deposition modeling (FDM) are used in this approach to create structures with sizes over 200 μm. In this method, the desired structure is created layer by layer from polymer powder.[21] Long et al. created a single layer of chitosan-hydrogel by 3D printing for wound dressing. However, its resolution was not less than 250 μm in contrast with a 2 μm cell size.[22] Ahmed et al.[23] added some graphene oxide to the chitosan hydrogel 3D-printting scaffold to enhance the rheological behavior. Chen et al. could improve the resolution of a 3D printed ceramic bone scaffold with fibers of 200 μm width. But this size of fibers is still far away from the native ECM fiber size.[24] Serra et al.[25] tried to decrease the fiber size, and they used a 3D printing concept to create a 3D structure made of polylactic glycol acid. The resulting structure had interconnected cavities. The diameter of the injected fibers does not seem to be controllable, varying between 70 and 150 μm. The other concept for the production of scaffolds with precise architecture is lithography, divided into two main categories, photolithography and soft-lithography.[26] Weiß et al.[27] used stereolithography with many types of polymers and biomaterials like acrylic, ZrO_2, gels, organic ceramic, polyesters, and gelatin to create different types of scaffolds. Serien and Sugioka[28] implied a multiphoton femtosecond laser to create a proteinaceous microstructure and a resolution of 3 μm. Claeyssense et al.[29] also used this method to create a copolymer of caprolactone and trimethyeneca bromate scaffold with a feature size of 15 μm. de Amorim Almeida and da Silva Bártolo[30] created a 3D pore medium of PDLLA mixed with fumaric acid monoethyl ester as a photo cross-linkable agent with a pore size of 400 μm. Yang et al.[31] used a bilayer microembossing technique to produce a 3D scaffold layer by layer. This method is basically based on microembossing of a heated layer of PCL polymer between two PDMS molds. To produce polymer layers, originally one single mold and later on two molds were used. To perform the embossing operation, the layer needed to be heated to around 220 °C. In the Yang setup, dimensions of the layers were 10 by 10 mm with a thickness of 120 μm and fiber size of 60 μm. In further research, Yang et al.[32] used replica molding to make micro- and nanopatterns with Diatom Bio Silica. They replicated this polymer on polydimethylsiloxane (PDMS) with an array of 80 μm upset disks with nanoholes to enhance the cell attachment. They replicated this complicated pattern based on a combination of PDMS molding and UV-curable noa-60. In the Gallego molding process, an initial layer was fabricated between a PDMS mold and a hot glass film. PCL was initially dissolved in tetrahydrofuran and dimethyl sulfoxide. By spin-coating, this solution was subsequently spread on the surface of the PDMS mold. At a later stage, the excessive solution was squeezed out by placing a hot glass film on top of the previous setup. The final structure was a monolayer made up of some flat square-shaped close-loops.[33] Ermis et al.[34] indicated that cell−substrate interactions played an important role in biomaterials and tissue fabrication. They showed the effect of dimensions and hydrophilicity of a scaffold with a repetitive pattern of square prisms on the cell body and nucleus deformation. Martella et al.[35] incorporated liquid crystalline (LC) elastomers with replica molding to create a nanostructure to improve cell attachment. LC polymers could be synthesized by chemically linking a mesogenic group to create a special polymer chain. These chains could be reshaped, thus achieving a dynamic scaffold during tissue development.

In this research, a new method of fabrication has been developed for the creation of a desired microdesigned scaffold stacked up layer by layer by applying two PDMS molds. This method is based on soft lithography and is capable of fabrication of various precise complex scaffold geometries having a fully interconnected structure with low fabrication cost. Using this method, many common obstacles like thickness limitation and incompatibilities with natural ECM can also be overcome. Resolution of this method is nearly 10 times that of the 3D printing method, which creates commercial designed scaffolds nowadays. So, on the micro-scale, it is possible to add characteristics like structural flexibility (for soft tissues) and also to control the cell colonies propagation strategy (see Figure 1).

2. MATERIALS AND METHODS

2.1. Concept of Fabrication. In order to fabricate scaffolds for tissue engineering, several functionalities of the fabricated tissue are required to be fulfilled: (i) maintaining a good mechanical strength even after grafting until the ECM is formed, (ii) good cell adhesion

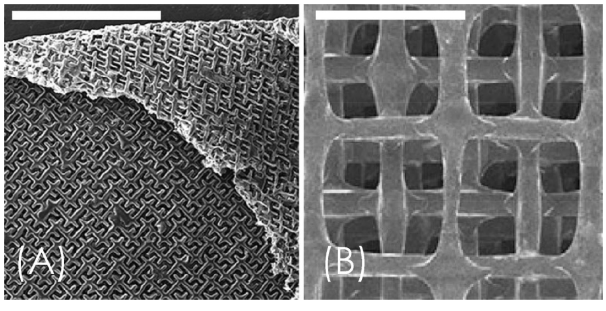

Figure 1. (A) A sample created with two PDMS mold replications (TPMR). (B) From a 3D printer with a fiber with a minimum diameter of 70 μm.[25] (The scale bar for both images is 500 μm.)

https://doi.org/10.1021/acsbiomaterials.1c00651
ACS Biomater. Sci. Eng. 2021, 7, 4763−4778

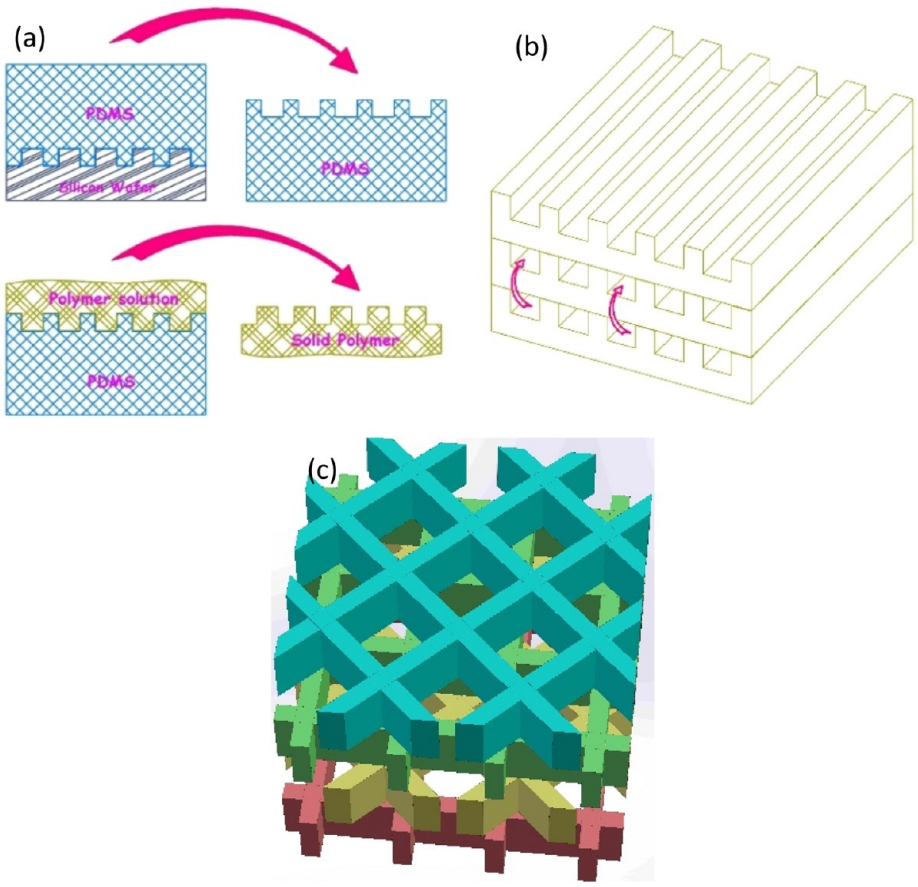

Figure 2. (a) Schematic of the steps of scaffold fabrication based on soft lithography. (b) Traditional scaffold building using soft lithography. Cells can be interchanged between the layers only from the channel entrance. (c) Transfer molding of polymer between glass and PDMS and final multilayer structure.

during culturing, and (iii) ease of cell migration through the depth of the fabricated scaffold.

Here, the method used (see Figure 2a) was based on soft lithography, for which the main steps are as follows:

- Step 1: creating a mother silicon wafer mold by masking, lithographing, and dry etching
- Step 2: pouring a formulated PDMS solution on the wafer and peeling off the resulting PDMS replica after curing
- Step 3: using the manufactured PDMS replica as a mold for fabrication of a polymeric layer

In traditional soft lithography, only "one segment PDMS mold" is present for the manufacturing of a scaffold by assembling the layers (Figure 2a). With this configuration, the resulting structure has no interlayer permeability, and the cell migration potential is nearly absent (Figure 2b). In another method of soft lithography, a replication takes place between one PDMS mold and a flat glass in order to reach the interlayer permeability. This method of fabrication produces a cross-linked layer with a closed-loop form that restricts the planar propagation of cell colonies and nutrition (Figure 2c). So the colonies form a spherical shape that is not suitable for sheet-form tissues like skin and cartilage. Generally, traditional soft lithography has not been a practical method for tissue engineering until now.

In the new method, it is proposed to perform the molding of the polymeric layer between "two segments of a PDMS mold", with each segment having its own specific canalized pattern (Figure 3a). This method has three main important advantages:

1. interlayer permeability of the final structure of the stacked-up scaffold and good cell migration between layers (Figure 3b)
2. significantly improved planar cell propagation in the canalized structure compared to closed-loop layers
3. easy accessibility to a wide range of scaffold designs (Figure 3c and d)

Using this method, after the layers have been cast, they can be stacked-up and sintered to form a complete scaffold with a desirable thickness. In Figure 4, the total process steps are shown in flowchart format.

2.2. Design of Scaffold. The study of this new fabrication method first requires the design of a preliminary mold to cast the layers with adequate fiber distribution. In this regard, some constraints should be taken into account:

(a) The straight fibers have minimum engagement of the polymer with PDMS; thus, separation of the layer from the mold segment is easier.

(b) Nonstraight fibers are more stable under compressional force, and the zig-zag fiber has mechanical flexibility for a soft tissue scaffold.

(c) The fiber spacing should correspond to the fibroblast cell size, used in skin production, being 2 to 3 μm when it is fully spherical and about 50 μm for a flattened cell.

(d) In silicon wafer lithographing and etching, the ratio of depth to width of the features must usually be kept under 4.[34] To be on the safe side, a ratio of 3 was selected. The maximum depth of etching was chosen to be 30 μm due to technical limitations. The approximate fiber width was chosen to be 10 μm.

(e) PCL was selected as the scaffold material, due to its flexibility.

To help find the best spacing for optimum cell adherence and test rate of penetration, the approach was to design various geometrical patterns on the same mold containing four different zones with different fiber spacings (20, 30, 40, and 50 μm). The dimension of 5 × 5 mm was arbitrarily chosen for each zone. This reduced the time and cost of mold fabrication. The zones were designed as shown in Figure 5.

https://doi.org/10.1021/acsbiomaterials.1c00651
ACS Biomater. Sci. Eng. 2021, 7, 4763−4778

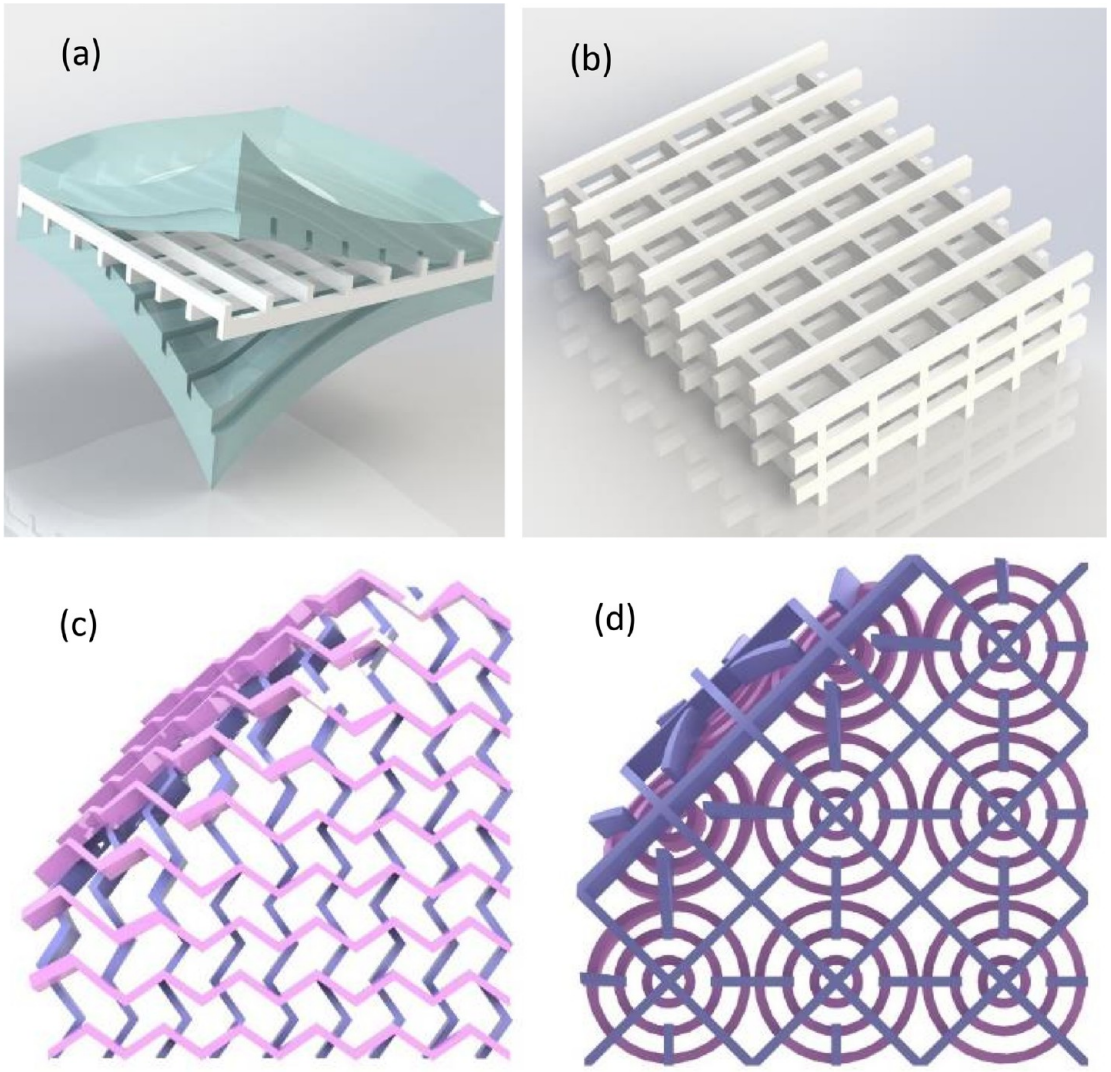

Figure 3. New method of fabrication with two segment PDMS mold. (a) Schematic of the two segment PDMS mold and the fabricated polymer layer. (b) Three stacked-up polymeric layers with interlayer permeability for cell migration. (c) Zig-zag double pattern. (d) Concentric circles double pattern.

Three different fiber forms are shown in Figure 6. The nonstraight fibers are more stable and can modify the mechanical behavior of the structure as well as cell development in 3D. Figure 6a shows the "simple zig-zag" structure with a fiber width of 8 μm and spacing of 32 μm. Figure 6b illustrates the "branched zig-zag" structure with a fiber width of 8 μm and spacing of 55 μm. The branches help the cells to create cell bridges between two neighbor fibers. This structure is 4 times more flexible than the simple zig-zag theoretically. Figure 6c represents the "straight dendritic" fibers with a width of 10 μm and spacing of 85 μm. To help the cells fill a channel, some cross-shape branches have been added to the main fiber that reduce the wall-to-wall distance. The layer thickness was considered to be 60 μm, similar to the previous multipore size pattern.

For culturing human dermal fibroblasts (HDF), due to the intrinsic elasticity nature of the skin, a zig-zag pattern was the most suitable pattern. Considering this concern, a modified zig-zag pattern, with a fiber thickness of 16 μm and a large spacing of 85 μm, allowing the HDF cells to penetrate deep into the scaffold thickness, was designed (Figure 6c).

The differences between linear and zig-zag fibers are as follows:

- Straight fibers exhibit much more rigidity than zig-zag fibers when they are stretched in the fiber direction.
- Straight fibers exhibit much more permanent plastic deformation than zig-zag fibers. Zig-zag fibers have a kind of accordion shape, and that is the main reason for it to retain its original shape.
- Straight fibers, due to their low rigidity in bending, are more susceptible to plastic deformation and folding than zig-zag fibers when they are subjected to sintering compressive pressure.

The importance of having tentacles and dendrites is, where for technical reasons, such as for increasing porosity, distance between two adjacent fibers is going to be extended. In such a case, cell culturing becomes a problem. To overcome this problem, the best common way is to fill the space between these two with some tentacles or dendrites.

2.3. PDMS Mold Preparation. A 4-in. silicon wafer disk was used to fabricate the two-segment PDMS molds and spin-coated to create a 30 μm KMPR-1025 layer. Then, the wafer was placed under a UV masked beam to create the desired pattern. The uncured area was washed out, and two patterns with 30 μm height remained as the mother mold (Figure 7). The other three nonstraight fiber patterns were created by SU-8 2010 lithography on a 2-in. silicon wafer, then dry etched down to 30 μm, and the photoresist was stripped. Finally, the wafers were treated by chromium to smooth the surfaces and remove micrograss.[36] The excess of all wafers was trimmed by laser, so it was possible to place them precisely at the engraved aluminum supporting base (Figure 7c). The modified zig-zag pattern, with two

https://doi.org/10.1021/acsbiomaterials.1c00651
ACS Biomater. Sci. Eng. 2021, 7, 4763−4778

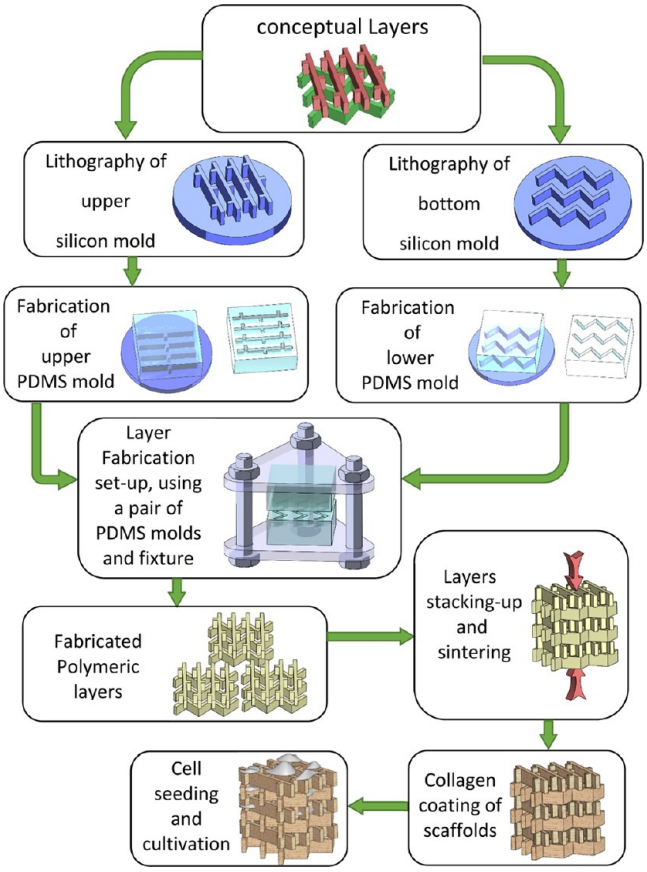

Figure 4. Manufacturing process chart from design to cell cultivation.

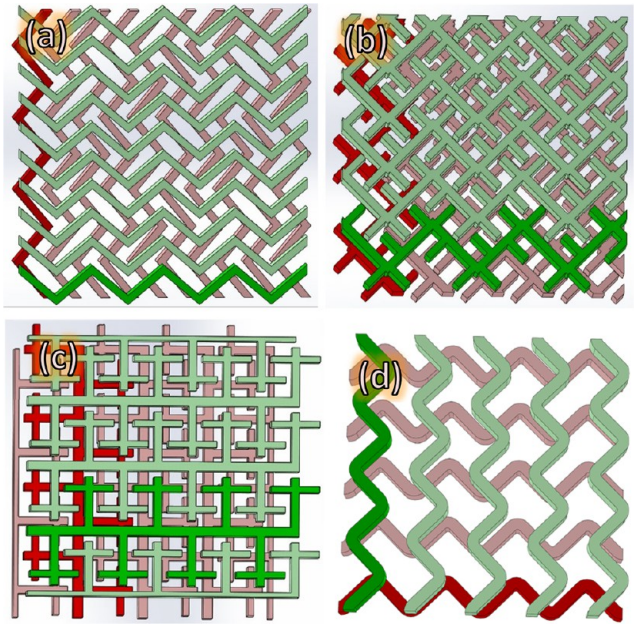

Figure 6. Schematic of the designed scaffold structure with special fiber forms and overall dimension of 20 × 20 mm. Green fibers represent the top level woofs, and the red one represent warps of one polymeric layer. The highlighted woof and warp in each picture can help to understand the pattern design concept. (a) Simple zig-zag fibers. (b) Branched zig-zag fibers. (c) Straight dendritic fibers. (d) Modified zig-zag pattern for HDF cell culturing.

patterns on one wafer, were created by depositing of a proprietary photoresist layer on a 3-in. silicon wafer (Figure 7d).

To avoid PDMS leaking during casting in the cavity when pouring PDMS on the silicon wafer, a square-shaped polytetrafluoroethylene (PTFE) wall barrier precisely aligned with the center of the pattern was designed. The walls were kept firmly tight to the silicon surface using an appropriate fixture (see Figure 8). The assembly of wafer and fixture was washed by acetone followed by methanol to remove all contaminations. Then, a 10% hexamethyldisilane solution was sprayed on the wafer surface to cause PDMS to be peeled off more easily. To fabricate the PDMS molds, Silgard−184 was used, comprising two components mixing A and B with a weight mixing ratio of 10:1. For this purpose, the PDMS paste was gently mixed and placed in a vacuum under a pressure of 10 Pa for degassing. The paste was then poured into the mold cavity. For curing, the whole system including fixture, silicon wafer, and PDMS molds was placed in an oven heated at 70 °C for 90 min to be cured perfectly. The PDMS layers were then peeled off from the silicon wafer. The thickness of the quad-zone PDMS pattern was 6 mm, while the thickness of the three nonstraight forms was about 1.5 mm.

2.4. Single Layer Fabrication. This method is based on casting a formulated polymeric solution of PCL between the two segments of PDMS mold. After casting and solvent vaporization, a thin layer of solidified PCL polymer is created. Three types of polymers consisting of PCL, PLA, and PVA are used in the present study.

(1) PCL: Sigma Aldrich 440744 with a molecular weight of 80 000.
(2) PLA: Sigma Aldrich 38534 with a molecular weight of 60 000.
(3) PVA: Sigma Aldrich 10853 with a molecular weight of 47 000.

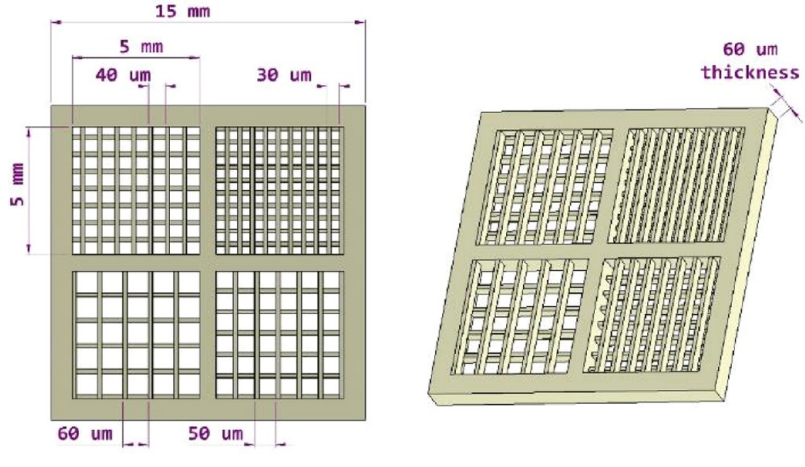

Figure 5. Schematic of the designed scaffold structure with dimensions. Fibers are magnified to indicate the zones and fiber positions.

https://doi.org/10.1021/acsbiomaterials.1c00651
ACS Biomater. Sci. Eng. 2021, 7, 4763−4778

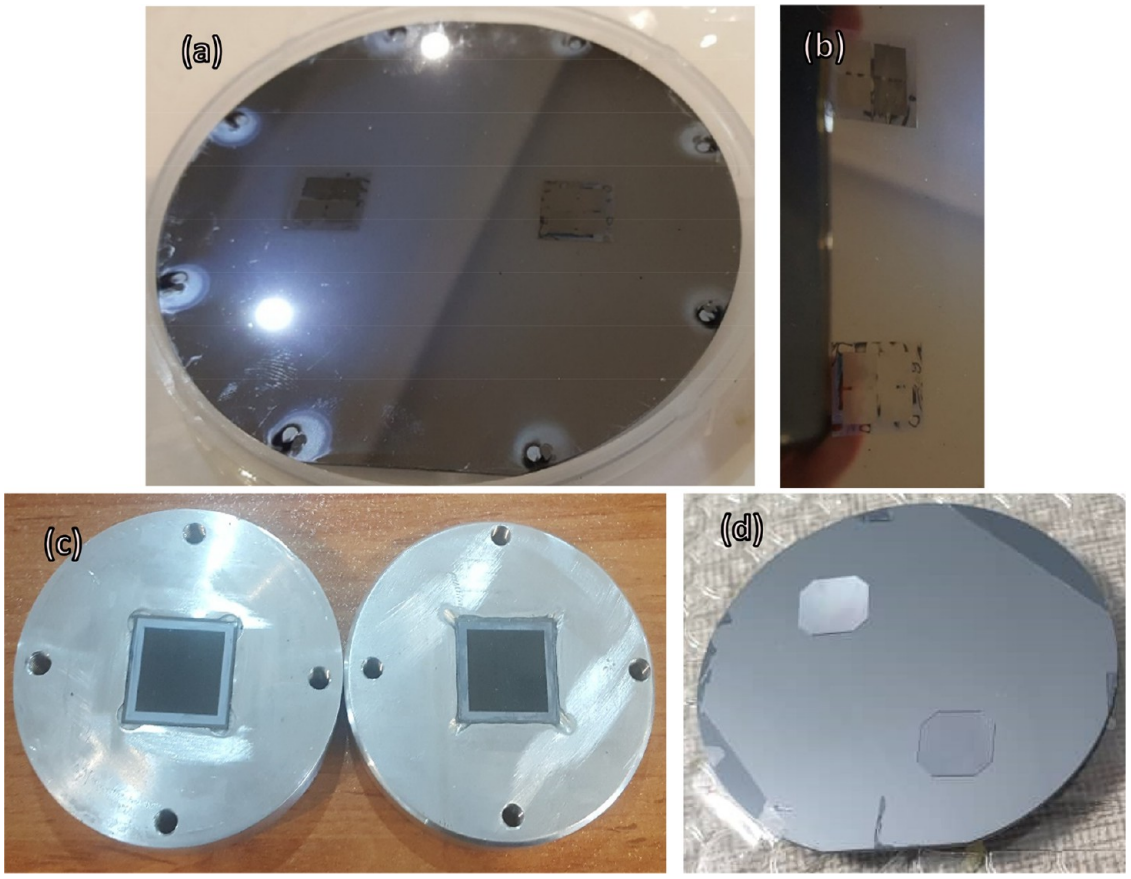

Figure 7. (a and b) Two patterns have been created on a 4-in. silicon wafer, each one consisting of four different zones. (c) Zig-zag and branched zig-zag patterns mounted on an aluminum support by silicon paste to protect the wafers from breakage when PDMS is peeled off. (d) A 3-in. wafer with two similar modified zig-zag patterns.

The best solvent for PCL and PLA as well as the copolymer of these two types is chloroform, and it is widely used for ES (refs 37, 38). Four different solutions have been prepared to examine the feasibility of this method. The basic solution for the present research was PCL-chloroform. PCL is very flexible and suitable for fibroblast cell culturing to produce skin tissue. The other solution was PLA-chloroform that produces a rather rigid polymeric scaffold compared to PCL. To approve the capability of this method to fabricate a scaffold with a wide range of polymers, a water-based solution has also been studied. For this purpose, PVA powder has been dissolved in distilled water. The ratios of polymer to solvent are listed in Table 1.

To fabricate different layers, a specific fixture was made integrating three sets of locking screws to tighten the two platens. The solidifying fixture should be tightened firmly to avoid the creation of "closed windows," which drastically reduce the permeability during cell culturing (Figure 9). The platens were made from clear polyacrylic, allowing for the solidification process to be visible (Figure 10a).

After the design and manufacture of the drying fixture, the layer fabrication started:

- The segments were assembled in the fixture cavities in the right orientation.
- A specific amount of polymer solution was injected on the top mold in the middle zone of PDMS with a glass syringe. The volume of injected polymer solution was about twice the vacant volume between the segments. The excess solution was squeezed out when the mold segments were assembled (Figure 10b).
- The top platen was placed on the lower one and hand-tightened gently so that the extra solution was squeezed out, thus filling the cavity between the mold segments.
- Due to the high wettability of chloroform on PDMS, the capillary forces pull the solution into the cavities.
- In the case of water-based solvent, the solution between two molds has been pressurized and pushed to the channels of PDMS mold, filling all the cavities.
- Next, the screws were tightened.
- After 5 to 6 h, the solidified layer was ready to be extracted.
- In the PVA−water solvent, more than 24 h was needed so that water completely vaporized.
- The fixture was unscrewed. The platens were depressurized, and the upper platen was separated from the lower one.
- The upper segment was then separated by precise lifting, starting from one corner.
- After removing the upper segment, the layer was peeled off gently from the lower segment
- The produced layer was stored on a glass slide (Figure 10d and f). Pictures of the process are shown in Figure 11.

2.5. Layer Sintering. The thickness of the produced layers was between 0.05 and 0.06 mm. This low thickness was not suitable for tissue engineering where preferable thickness is usually around 1 mm. To overcome this obstacle, it was essential to sinter numerous layers to create a suitable thickness. The sintering process consists of the following:

i. Stack up dried layers in a specific aligned sequence

- Rotate the quad-zone pattern samples to the same orientation on a glass slide by means of forceps under an optical microscope
- Carefully put the layers one by one on the bottom platen of the sintering fixture; the plus sign of each new layer must be aligning with the previous (Figure 12b)
- Put a droplet of methanol on all stacked layers to prevent any relative planar movement during clamping (Figure 12c)

ii. Place polymeric layers in a clamp device; apply a proper pressure (0.8−1.0 Mpa)

https://doi.org/10.1021/acsbiomaterials.1c00651
ACS Biomater. Sci. Eng. 2021, 7, 4763−4778

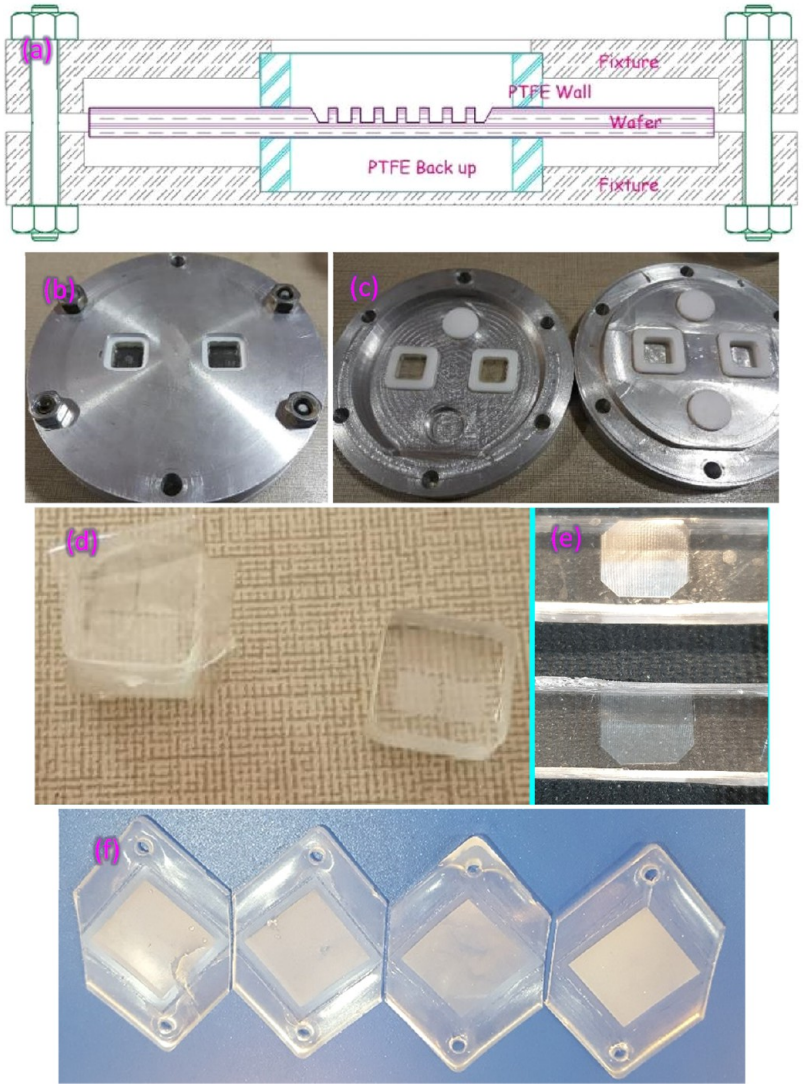

Figure 8. (a) Schematic of the PTFE fixture (b) Complete closed system for casting PDMS on silicon wafer including PTFE wall barriers. (c) Two platens of fixture (open system). (d) Quad-zone PDMS molds. (e) Modified zig-zag PDMS molds. (f) Zig-zag, horned zig-zag, and dendritic molds.

Table 1. Different Solvents Used in Polymer Solution

name	polymer	solvent	polymer ratio mg/cc
S1	PCL	chloroform	18−30
S2	50% PCL−50% PLA	chloroform	23
S3	PLA	chloroform	21
S4	PVA	distilled water	16

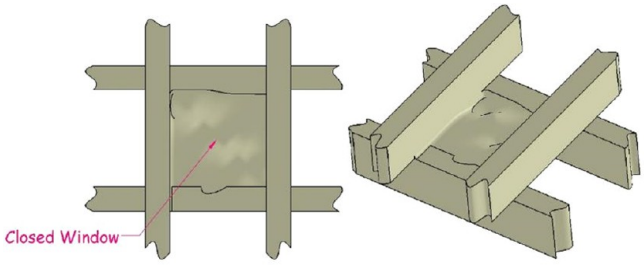

Figure 9. Concept of closed window.

A special clamping device with the following characteristics has been made:

- Six places to be able to sinter six scaffolds simultaneously
- Notched silicon rubber pads with 6 mm thickness to apply sintering pressure uniformly and also to prevent the folding of exterior fibers
- Three screws to maintain the pressure during sintering process (Figure 12a)
- Some stoppers to standardize the amount of compactness of the rubber pads and thus the compression stress (Figure 12d)

Hint: the sintering pressure was controlled by means of the elastic modulus of the rubber pads (4 Mpa) and the amount of compressional strain (25% of 12 mm total height equal to 3 mm compactness)

iii. Insert the clamp device in an oven heated at 40 °C for 3 h

- Due to the viscioelastic behavior of PCL, it took time to strengthen the bonds at the contacting junctions.
- A higher temperature leads to stronger bonding but increases the risk of structural collapse.

iv. Open the clamp device and separating the sintered layers (Figure 12e).

Finally, it was concluded that the strength of sintering junctions was lower than the perfect internal layer junctions between the woofs and warps.

The shear strength of two sintered layers was measured to be around 1.4 MPa. That is roughly around 1/4 of PCL shear strength.

2.6. Cell Culturing. All scaffolds were treated with NaOH solution to make the surface hydrophilic.[39] Each scaffold had four

https://doi.org/10.1021/acsbiomaterials.1c00651
ACS Biomater. Sci. Eng. 2021, 7, 4763−4778

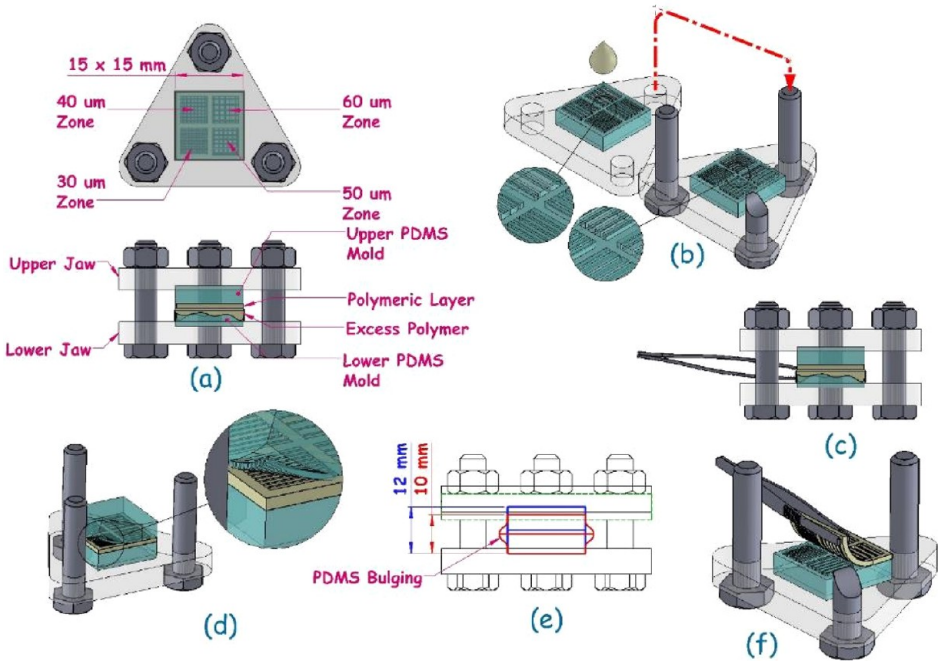

Figure 10. Process of replica molding of the polymeric layer between the two segment PDMS mold including the designed fixture. (a) Drying fixture top and side views. (b) Pouring the polymer solution and closing the fixture. (c) Removing excess polymer. (d) Removing the top PDMS platen starting form one corner. (e) Applying a 2 mm squeeze to pressurize the PDMS segments. (f) Peeling off the casted polymeric layer.

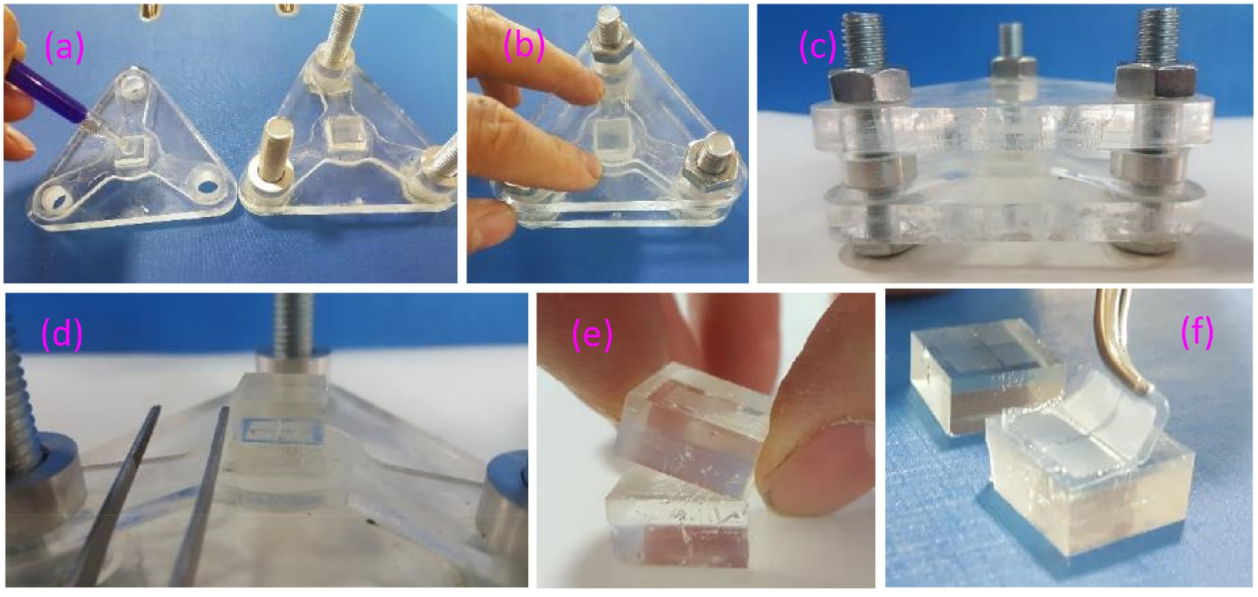

Figure 11. Pictures of the layer fabrication process. (a) Injection of polymer solution by syringe. (b) Closing the fixture. (c) Drying the layer. (d) Removing the top platen. (e) Removing the top PDMS. (f) Peeling off the layer from the lower platen.

zones with different spacing; thus cell culturing could be evaluated to find the most optimal spacing. Considering the risk of contamination, at least three samples, each consisting of three layers, were fabricated for each type.

For culturing purposes, the samples were initially disinfected with ultraviolet germicidal irradiation (UVGI). They were then placed evenly in an untreated Petri dish and put in an incubator in an atmosphere of 5% CO_2 heated at 37 °C. A specific amount of cell culture medium, containing 40 000 L929 mouse cells (Pasteur Institute of Iran), was injected into each sample. After 2 days, samples were removed by forceps one by one, and the number of free cells in the leftover serum was counted. The samples were then monitored with an optical microscope during the culturing process.

When the culturing process was finished, the samples were washed to remove nonadhered cells and then submerged in 8% glutaraldehyde for 2 h, thus killing all the live cells and fixing stocked cells. The samples were finally washed with distilled water and dried in an oven at 37 °C.

The method of culturing of human dermal fibroblast (HDF) on a modified zig-zag pattern scaffold was similar to that of L929. However, after cultivation, the samples were painted with a fluorescent dye, Acridine Orange Propidium Iodide, for observation of the colonies under an optical fluorescent microscope.

https://doi.org/10.1021/acsbiomaterials.1c00651
ACS Biomater. Sci. Eng. 2021, 7, 4763−4778

Figure 12. (a) Aluminum sintering fixture with six sintering cavities. (b) Placing layer by layer of scaffold and aligning them with each other. (c) Adding some methanol to fix the layers relatively. (d) Sintering the fixture in closed position. (e) Peeling off the solidified layer.

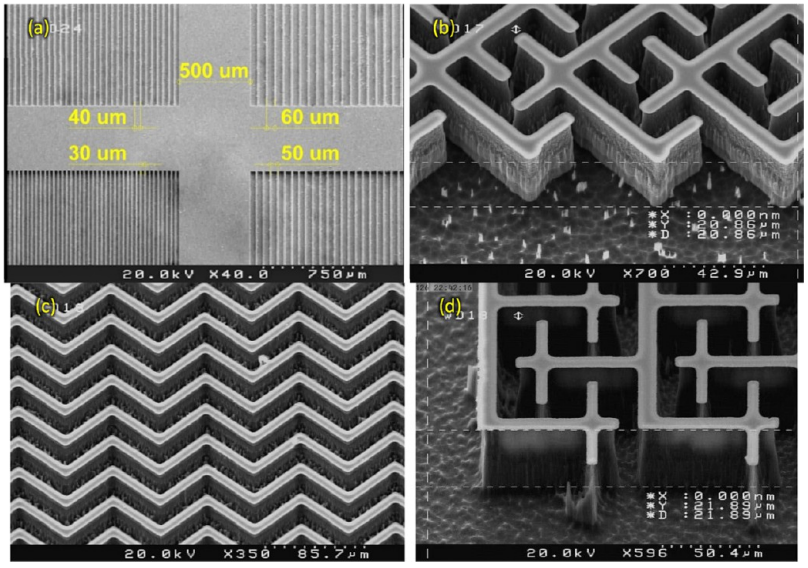

Figure 13. (a) General overview of four zones, center of pattern. SEM imaging of three silicon wafers with 45° inclination angle. (b) Branched zig-zag pattern. (c) Simple zig-zag pattern. (d) Straight dendritic fiber pattern.

3. RESULTS AND DISCUSSION

3.1. Silicon Wafer and PDMS. As the patterns are so fine, the quality of the produced quad-zone silicon wafer was evaluated by SEM imaging of wafer without metal sputtering (Figure 13a). As shown, the quality of fiber in the wafer was excellent, and also the spacing of fibers was precise. The vertical walls were completely smooth to make PDMS and the polymeric layer peeling off process easy.

There were also three nonstraight fiber patterns created by dry etching on three silicon wafers. To examine them, oblique SEM imaging was utilized with a 45° inclination angle (Figure 13b–d). The wafers were etched, in contrast with the previous one, to create the desired features with a certain height. The only single advantage of this method is the endurance of the mother mold to repeat PDMS replication many times. There were, however, some defects that make dry etching useless for this application:

(i) The vertical faces of walls were rough, making PDMS replication as well as separation of the polymeric layer from PDMS difficult.

(ii) The bottom surface plays an important role in wiping out polymer solution, preventing the window blocking membrane to be formed (Figure 9). But a rough etched bottom makes the crest of the PDMS mold rugged (two mutual rugged surfaces of PDMS molds entrap the polymer solution, and after solidification, an unwanted polymer membrane remains that reduces the interlayer permeability).

(iii) Unavoidable undercuts of silicon during dry etching were clearly detectable, especially at the branch ends in Figure 13b and d. To remove the micrograss, the wafer with a dendritic pattern was treated by chromium, which further intensifies the undercut (Figure 13d). The residual photoresist

https://doi.org/10.1021/acsbiomaterials.1c00651
ACS Biomater. Sci. Eng. 2021, 7, 4763–4778

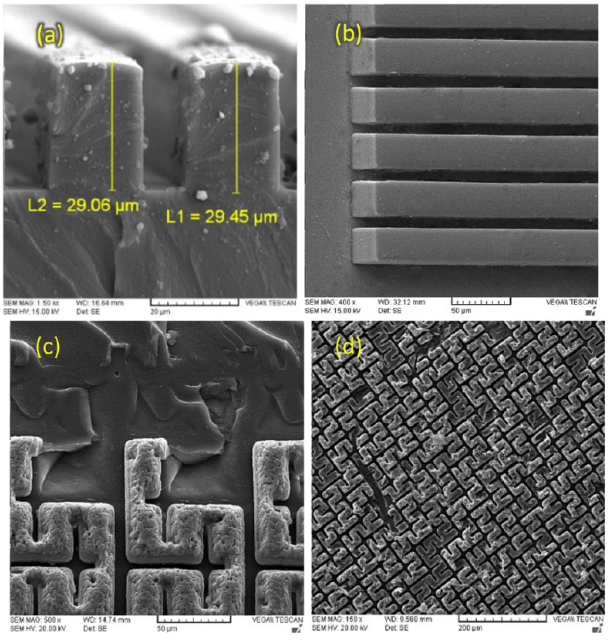

Figure 14. (a) Cross-section of PDMS and height of the features. (b) 40 μm spacing zone. (c) Dendritic pattern with slight deviation from right angle view. (d) Branched zig-zag PDMS overview.

showed the correct pattern, and some portions of wall volume were missed in comparison with the photoresist. These undercuts make both PDMS and polymer detachment hard or even impossible.

Considering the aforementioned issues, it is recommended that a photoresist with a strong bond with the silicon substrate that builds up the features is the best choice for creation of the mother mold.

To evaluate PDMS replication of the quad-zone straight pattern, two different imaging methods were used. The first one was the image of a cross-section cut, and the other was the image of PDMS in a slanted (45°) position. This created the possibility to check the pattern and height of PDMS features simultaneously. In Figure 14a, the real height of the features is shown that was near the theoretical height of 30 μm. In Figure 14b, oblique imaging was utilized to evaluate the quality of the replicated PDMS. In the detailed oblique images, the quality of PMDS features and smoothness of all faces are perfect, and PDMS filled all the mother silicon wafer features well. The height of the feature in the 45° slanted form was 21.60 μm, and by dividing to cos(45°), the real height of 30.45 μm was obtained. All the wafer and PDMS evaluations for the quad-zone straight pattern showed that the replication of PDMS was well performed, and no imperfection was observed in the PDMS mold.

As previously expected, the roughness and undercuts of silicon caused PDMS to be difficult to peel off, and in some cases, a rupture took place. An overview of the dendritic pattern PDMS is shown in Figure 14c. It shows the features in more detail in which half of the wall height had a smooth surface while the other half at the end was rough with some portions of the PDMS feature dismissed and stuck to the mother silicon mold. Both the undercut and roughness of silicon walls at the bottom of the wafer caused this rupture. In the branched zig-zag pattern (Figure 14d), the feature rupture is more obvious, although more than 50% of the PDMS features' height was generally intact.

3.2. Single Layer Fabrication and Sintering. Figure 15a shows perfect sharp edge fibers and open windows. Figure 15b demonstrates some burrs around each window. In Figure 15c, there were some ruptured membranes that can help to estimate a thickness lower than 1 μm. Figure 15d and e and f show the perfect structure of the polymeric layer with a quad-zone pattern and that the process of fabrication was well optimized. All windows are fully open, and fiber thickness and cross section are as well.

SEM images of other types of polymer have been shown in Figure 16. Figure 16a and b show the sample with 50% PCL–

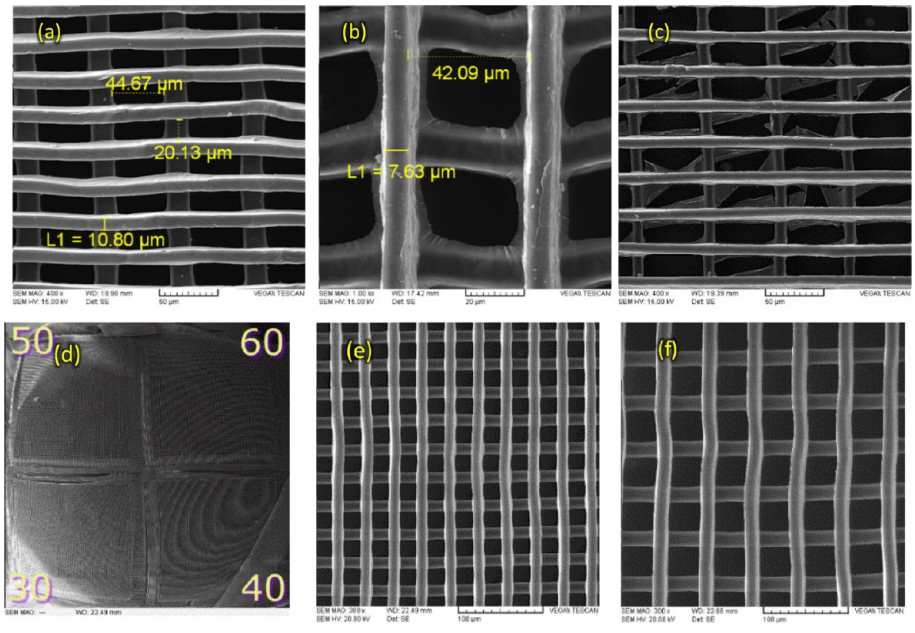

Figure 15. (a) Warp spacing is 30 μm and woof is 50 μm. (b) 40 μm spacing. (c) Zone with 40 μm warp spacing and 60 μm woof spacing. (d) Sample with equal spacing of warps and woofs with a 25 mg/cc solution. (e) 30 μm spacing perfect structure. (f) 50 μm-spacing.

https://doi.org/10.1021/acsbiomaterials.1c00651
ACS Biomater. Sci. Eng. 2021, 7, 4763–4778

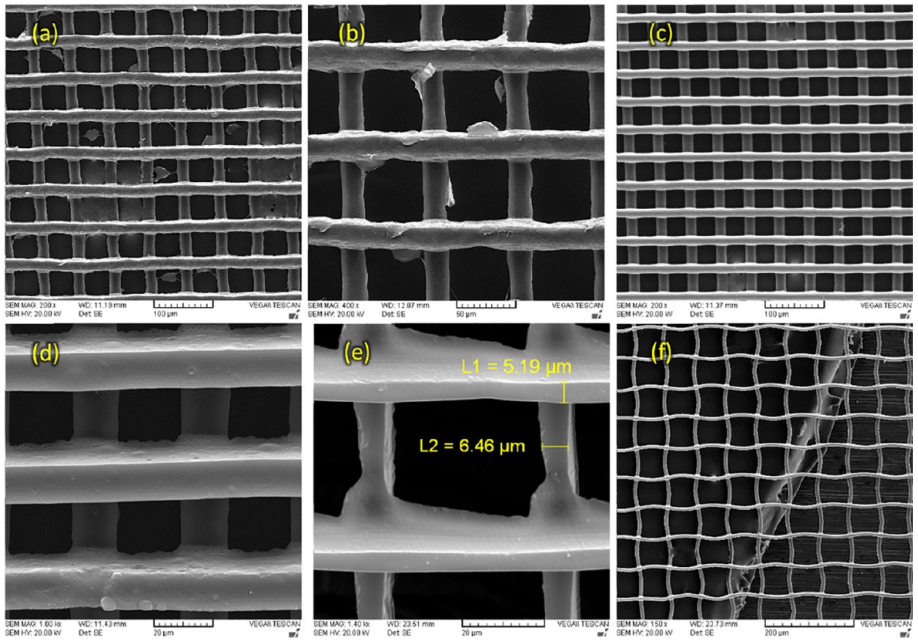

Figure 16. SEM imaging of other types of polymer (PLA, 50% PLA−50% PCL, and PVA) molded with four-zone basic mold. (a and b) 60 μm zone with 50% PCL-50% PLA. (c) 50 μm spacing with PLA. (d) 30 μm spacing with PLA. (e) 40 μm spacing with PVA. (f) 50 μm spacing with PVA.

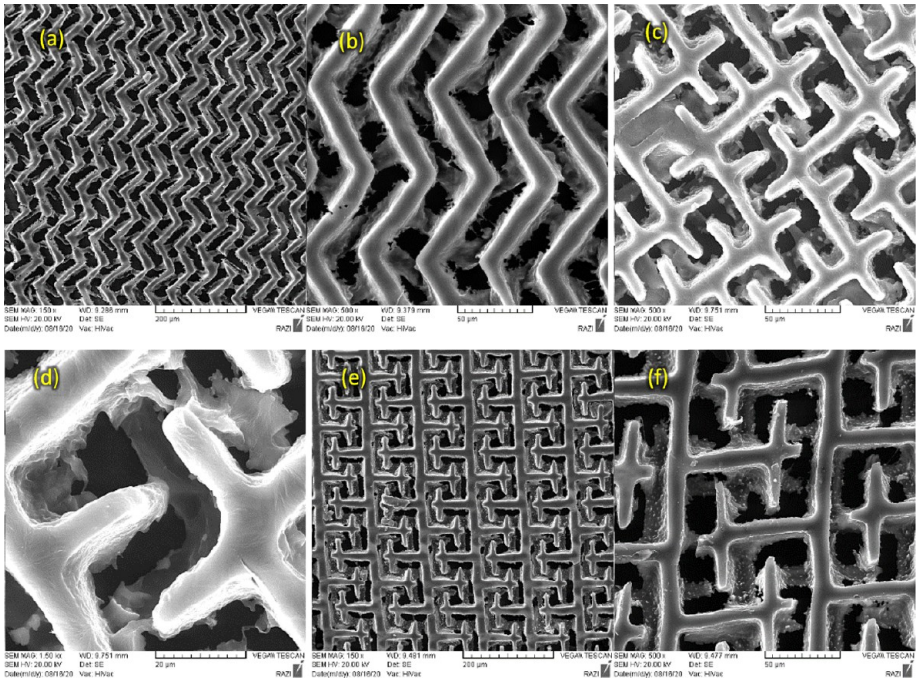

Figure 17. (a and b) Simple zig-zag fibers. (c and d) SEM image of branched zig-zag pattern. (e) Overview of the dendritic polymer layer. (f) Details view of dendritic fibers.

50% PLA (S2). This sample has an acceptable window opening, and the fibers are straight-line, having a good uniform thickness in different spacing zones. The fibers in this sample are straighter than those in PCL samples due to the presence of PLA that increases the rigidity of fibers. Elective SEM images of PLA samples (S3) have been illustrated in Figure 16c and d. The main characteristic of these images was the straightness and sharp edge of the fibers. The fibers were extremely rigid, and no distortion has been observed in their network. Also, the opening percentage was near 80%. In Figure 16e and f, the structure of the PVA (S4) polymeric layer is shown. The opening percentage was completely 100%, and the fibers were very thin (5−6 μm), that is, near half of the theoretical value. This was due to a high shrinkage factor of the PVA solution solidification as well as the hydrophobicity of PDMS mold walls. When the solvent used was chloroform, which improves wettability, the solution during solidification tended to stick to surfaces of PDMS and made fully filled fibers in PDMS channels. But in this condition, the solution shrank

https://doi.org/10.1021/acsbiomaterials.1c00651
ACS Biomater. Sci. Eng. 2021, 7, 4763−4778

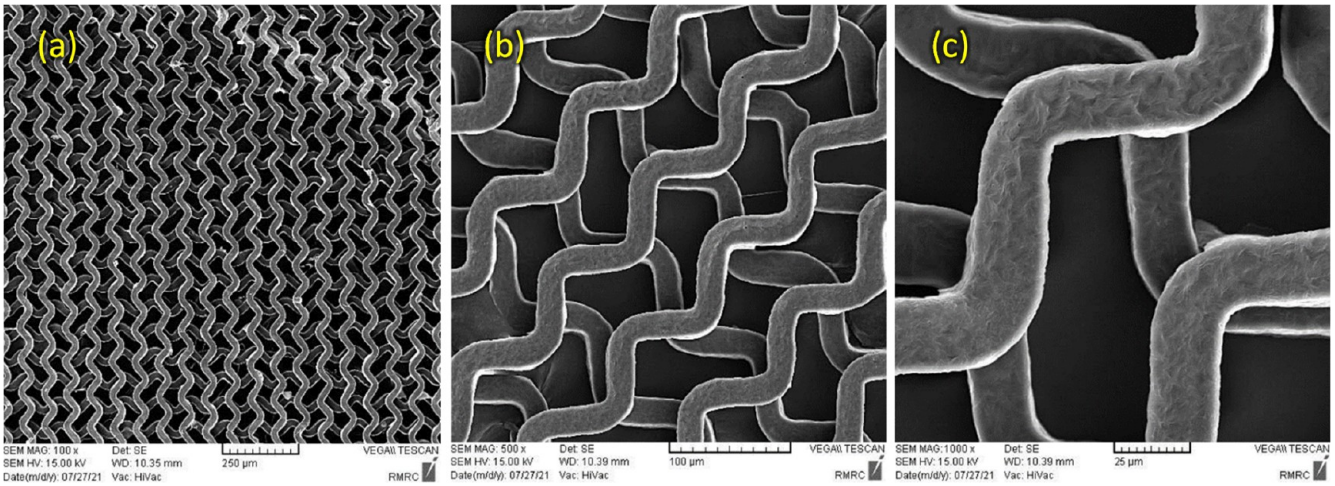

Figure 18. SEM images of two samples of modified zig-zag structure with different magnifications. (a) 100×, (b) 500×, (c) 1000×.

Table 2. Comparison of Different Patterns

fiber shape	thickness modality[a]	max fiber spacing[b]	approx. max porosity[c]	flexibility[d]	collapsing resistance[e]	applications	description
straight	unithickness fibers	70 μm	80%	bad	bad	bone	rigid scaffolds for hard applications and poor for vascularization; poor collapsing strength (not suitable for cartilage)
	bithickness fibers	70 μm	77.5%	very bad	fair	blood vessel	
zig-zag	unithickness fibers	80 μm	82.5%	great	good	epidermis	flexible structure with wide range of mechanical properties for rather flexible tissues
	bithickness fibers	80 μm	80%	good	great	dermis blood vessel cornea	
zig-zag branched	unithickness fibers	130 μm	87.5%	excellent	good	dermis	extra-flexible scaffold with capability of vascularization for thick tissues (more than 2 mm)
	bithickness fibers	130 μm	85%	great	great	parenchyma	
straight dendritic	unithickness fibers	170 μm	90%	mediocre	great	bone	poor flexible structure with excellent in vivo vascularization and osmosis nutrition of thick tissues; best choice for cartilage
	bithickness fibers	170 μm	87.5%	poor	excellent	cartilage cornea	

[a]In the unithickness modality, the widths of all fibers are identical. In a bithickness modality, with a specified repetition order, the width of that specified fiber is thicker than the previous ones. These wider fibers are included to increase the strength of the whole layer. [b]This column shows maximum spacing between two adjacent fibers while cell bridging or culturing is possible. Beyond these limits, cell culturing will be less likely and even not possible. [c]This column is an indication of the lattice hollowness. More porosity shows greater cell absorption capacity and ease of cell penetration during cell culturing. [d]This column shows elasticity of the pattern. Skin tissue application requires extremely flexible structures in all directions. [e]This column shows structural resistance against external pressure. A structure with poor structural resistance is not suitable for a skin graft as a slight external pressure can result in crushing the whole transplanted patch, during its rather long healing time.

Table 3. Fabrication Optimization Technique

	optimization parameters			
diagnose	polymer solution rheology	pre amount of polymer solution	clamping pressure	clamping sequence
partially closed windows with remaining burrs	make the solution thinner		small increase in pressure	
large regional closed windows	make the solution thinner	decrease the amount of droplet and spread it on the PDMS mold	large increase in clamping pressure	two molds' surfaces gradually come into contact with each other
hollow or locally thin fibers	make the solution thicker	increase the amount of predroplet solution	increase the clamping pressure	
cross-sectional deformed fibers	make the solution thicker		decrease the clamping pressure to prevent PDMS mold deformation	simultaneous contact of two PDMS mold surfaces
planar distortion of fibers	make the solution thinner	decrease the amount of polymer solution	decrease the clamping pressure	simultaneous contact of two PDMS mold surfaces

and was detached from PDMS walls, then forming narrow fibers.

Although the quality of nonstraight pattern PDMS molds was not high for the mass production of layers, PCL (the

https://doi.org/10.1021/acsbiomaterials.1c00651
ACS Biomater. Sci. Eng. 2021, 7, 4763−4778

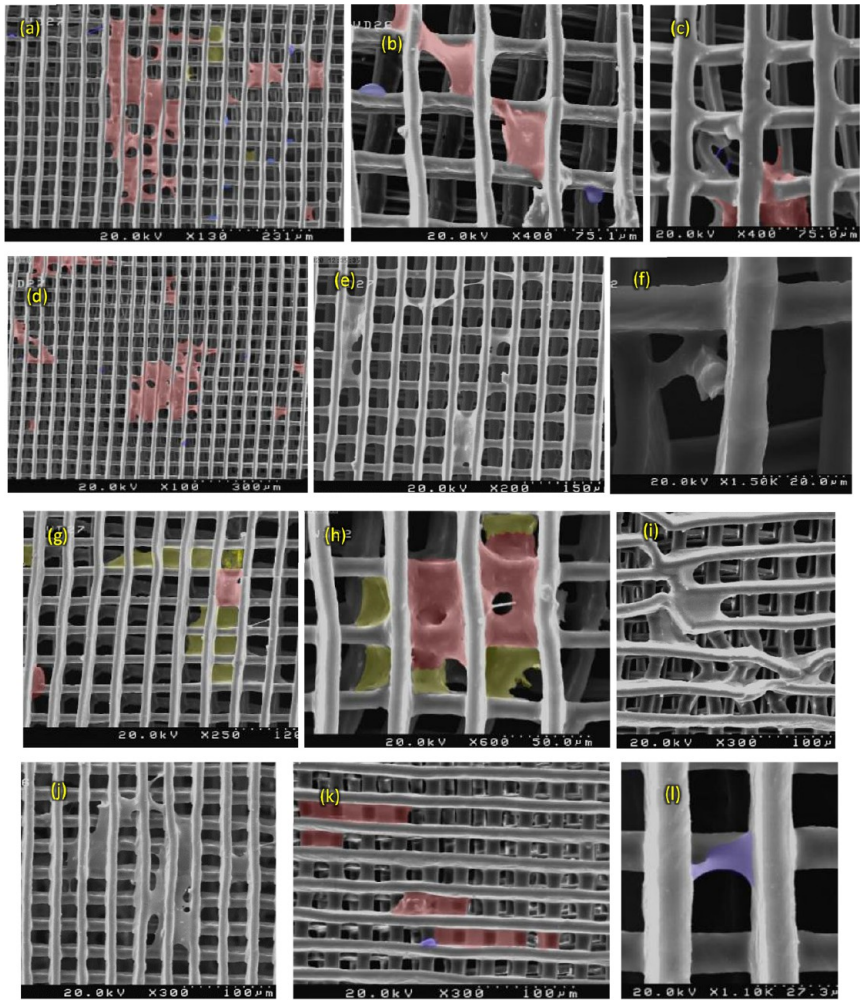

Figure 19. (a) 60 μm spacing zone with colonies and stuck single cells. (b) 60 μm spacing, one single cell and two linked colonies. (c) 60 μm spacing, one small colony at the top layer in horizontal channel. (d) 50 μm spacing, one major colony and six small colonies. (e) 50 μm spacing, six small colonies at the top. (f) 50 μm spacing, a single cell at the second layer. (g) 40 μm spacing, two large colonies in the second layer, one small colony at the top. (h) 40 μm spacing, an excellent multilayer colony that well adhered to the scaffold. (i) 40 μm spacing, some colonies formed in the damaged fibers region. (j) 30 μm spacing, two major linked colonies and one small colony. (k) 30 μm spacing, two colonies aligned with top fibers. (l) 30 μm spacing, a single cell attached to a horizontal and vertical fiber.

mainly used polymer in this research) layer fabrication was performed for these types to examine the sensitivity of TPMR to the quality of PDMS and also the possibility of peeling off the polymeric solution when the structure is more complex than the straight type. Results are shown in Figure 17 for simple zig-zag, branched zig-zag, and straight dendritic forms. Figure 17a and b show the simple zig-zag fibers with appropriate windows opening. Warps and woofs can easily be seen. Fibers show some defects such as pits and discontinuities in some points. Figure 17c and d show the branched zig-zag pattern with a higher brightness to clarify the woofs and the warps. Figure 17e shows the overall dendritic pattern with perfect fibers and totally opened windows. Figure 17f shows details of dendritic fibers.

The general conclusions from replication of these three patterns by using a dry etched wafer can be summarized as follows:

(1) This method is a powerful tool in producing various designed scaffolds.

(2) The fiber filling of the PDMS mold as well as the percentage of opened windows were satisfactory.

(3) Considering the detachment of the polymer layer from the PDMS mold, it was realized that a branched zig-zag pattern was the most flexible form, followed by a simple zig-zag pattern, while the dendritic form had rather rigid behavior. The zig-zag form on the microscale can make the structure flexible even with a rigid polymer such as PLA. Due to this advantage, expensive natural polymers like collagen and elastin can be replaced with inexpensive synthetic polymers for soft tissue engineering.

Figure 18 shows some polymeric samples with modified zig-zag patterns designed for HDF cell culturing. For these samples, the fiber thickness was around 16 μm, and the fiber spacing was around 90 μm, which are consistent with the ideal dimensions. As seen, the fibers have rather sharp edges with almost no burrs and forming totally opened windows. These perfect patterns prove once again that the quality of the final polymeric layers directly goes back to the quality of the mother silicon wafer mold and is not related to the complexity of the pattern itself. With this philosophy, one can say that dry etching is not a recommended tool for TPMR application.

https://doi.org/10.1021/acsbiomaterials.1c00651
ACS Biomater. Sci. Eng. 2021, 7, 4763−4778

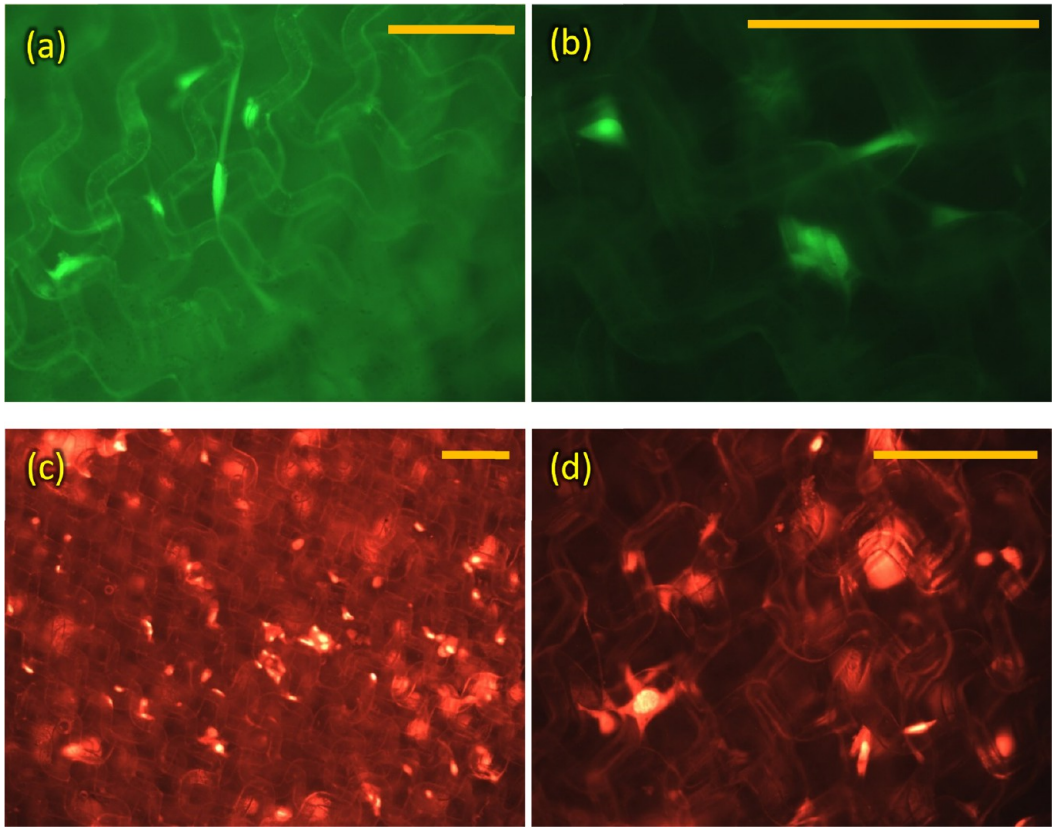

Figure 20. (a and b) One-day cultured sample painted with Acridine Orange. (c and d) Three-day cultured sample painted with propidium iodide. The scale bar is 200 μm.

Table 2 compares different structures and lists the advantages and disadvantages of each one so that an optimal structure can be found for each specific application.

3.3. TPMR Fabrication Process Optimization. Manufacturing optimization can include the following:

1. Concentration of the primary polymer used for molding
2. Amount of clamping pressure during the sintering
3. Closing sequence of the mold segments
4. Postreplication processes such as ultrasonic bath with diluted solvent and nanopowder etc.

On the basis of our numerous experiments, Table 3 shows few optimized parameters for some common defects.

3.4. Cell Culturing. SEM overview images were used to study how the cells attach to the scaffold and their colony shape forms (Figure 19). The most important problem here was to detect the cell colonies from various shape features of the scaffold which needs experience regarding this type of scaffold and cell colonization behavior. The best indications are listed below:

1. Closed windows belonged to a wide region and were rarely randomized. Cell colonies, however, formed randomly within the structure and closed some discrete windows.
2. If the channel between two neighboring fibers was filled, it indicated a cell colony. As shown in Figure 15, polymeric membranes could not come into the channel cavity in the fabrication process because of the presence of PDMS fibers during the solidification process of a layer.
3. The dusts and deformed fibers had sharp edges, unlike cell colonies which had smooth edges similar to an "elastic band" pulled from some points.

Unbound cell count was also used for evaluation in addition to SEM images. There were two samples for cell culturing: one sample with 12 000 unbound cells and the other with approximately 16 000. The total cell count was 40 000, so the bounding efficiency was 60%, which is acceptable for a three-layer scaffold.

The L929 cell culturing results showed that the cells stuck to the scaffold, proliferated, and formed colonies. Because of complete interconnection by horizontal and vertical channels, they had a good planar propagation. The size of cells was considerably smaller compared to channel size; therefore, in the first stage, a single cell adhered to a fiber wall, having a loose attachment. Its bonding became stronger by proliferation, development of colonies, and attachment to another surface. This development even caused some windows to be closed by a cellular bridge. However, for 50 and 60 μm spacing, cells could severely block the windows. Although "penetration in depth" of cells was significantly smaller than "planar propagation", it was better than the other methods of scaffold fabrication. For 30 μm spacing, almost all cells did not have a tendency to penetrate inside the scaffold, while for 40 μm spacing, there were some colonies observed in the second and third layers. Also, for 50 and 60 μm spacing, the penetration became more difficult due to a deficiency of specific surface area. Hence, the best choice here was 40 μm spacing (Figure 19h). Parameters such as using a bioreactor, static culturing, and long-term culturing would increase penetration depth, which need further research. Finally, it was found that 40 μm was the best spacing, and it is recommended as the basic value for the design of other types of scaffold in future studies.

https://doi.org/10.1021/acsbiomaterials.1c00651
ACS Biomater. Sci. Eng. 2021, 7, 4763−4778

Two scaffolds, each consisting of four layers of a modified zig-zag pattern, were used for culturing with HDF cells for cell penetration and their interaction study with the scaffold. The one-day cultured samples were painted with Acridine Orange, and the three-day cultured samples were painted with propidium iodide. Cell colonies were observed with an optical microscope. The results for the one-day sample are shown in Figure 20a and b. The results for the three-day sample are shown in Figure 20c and d. As shown, the cells have thoroughly penetrated and attached to the walls of the scaffold. Many colonies are detectable, especially when the culturing time was increased. The window size was large enough to let the cells penetrate deep inside the scaffold. Studying the pictures shows that corners are the best places for cell nesting.

4. CONCLUSIONS

The most prominent result of the present study is that the fabrication of scaffolds with two PDMS molds is a practical tool and that it can be commercialized through some appropriate modifications. Nonstraight fiber patterns (such as zig-zag, branched zig-zag, and dendritic patterns) were successfully produced even though the quality of the PDMS molds was not suitable. The poor quality of nonstraight fiber patterns was mainly related to the defects of the dry etched technique in manufacturing the mother silicon wafer instead of the photoresist deposition technique. As said, this latter tool brings about the possibility of constructing a wide range of complex geometries with heterogeneous and anisotropic characteristics, thus facilitating the production of a wide range of scaffolds for various types of body tissues. As said, the final structure can be constructed by augmentations of numerous layers on the order of 1-μm size. Furthermore, for proper implementation of the method, while having a robust scaffold, the sintering process needs to be improved. In addition, it was concluded that linear straight fibers are not suitable for scaffolds, because of their low contact areas needed for proper cell nesting. Additionally, this type of fiber has the least resistance under compression, causing the scaffold to be susceptible to collapsing. Thus, zig-zag fibers can be regarded as a more satisfactory replacement for straight fibers. From a culturing point of view, it was shown that the L929 cell bonding to the straight fiber scaffolds is rather acceptable. It takes a couple of hours for initial bonding, and if given enough time, cells will thoroughly penetrate through the whole structure. Moreover, it was concluded that 40 μm spacing is the best option for L929 cell culturing. For human dermal fibroblasts, modified zig-zag structures with 80 μm spacing (against 40 μm, optimum spacing for L929 cells) are a good option in terms of penetration characteristics.

AUTHOR INFORMATION

Corresponding Author

Majid Baniassadi − *University of Tehran, School of Mechanical Engineering, College of Engineering, Tehran 1417935840, Islamic Republic of Iran;* orcid.org/0000-0002-4434-082X; Email: m.baniassadi@ut.ac.ir

Authors

Hassan Najafi sani − *University of Tehran, School of Mechanical Engineering, College of Engineering, Tehran 1417935840, Islamic Republic of Iran*

Karen Abrinia − *University of Tehran, School of Mechanical Engineering, College of Engineering, Tehran 1417935840, Islamic Republic of Iran*

Nooshin Haghighipour − *National Cell Bank of Iran, Pasteur Institute of Iran, Tehran 1417935840, Iran*

Daniel George − *University of Strasbourg, CNRS, ICUBE Laboratory, 67000 Strasbourg, France*

Yves Remond − *University of Strasbourg, CNRS, ICUBE Laboratory, 67000 Strasbourg, France*

Complete contact information is available at: https://pubs.acs.org/10.1021/acsbiomaterials.1c00651

Notes

The authors declare no competing financial interest.

REFERENCES

(1) Mijatovic, D.; Eijkel, J. C.; van den Berg, A. Technologies for nanofluidic systems: top-down vs. bottom-up—a review. *Lab Chip* **2005**, *5* (5), 492−500.

(2) Huang, J. I.; Goldberg, V. M. Orthopedic applications of stem cells. In *Essentials of Stem Cell Biology*; Elsevier, 2009; pp 561−569.

(3) Huss, F. R.; Kratz, G. Mammary epithelial cell and adipocyte co-culture in a 3-D matrix: the first step towards tissue-engineered human breast tissue. *Cells Tissues Organs* **2001**, *169* (4), 361−367.

(4) Hutmacher, D. W. Scaffold design and fabrication technologies for engineering tissues—state of the art and future perspectives. *J. Biomater. Sci., Polym. Ed.* **2001**, *12* (1), 107−124.

(5) McClure, M. J.; Sell, S. A.; Barnes, C. P.; Bowen, W. C.; Bowlin, G. L. Cross-linking electrospun polydioxanone-soluble elastin blends: material characterization. *J. Eng. Fibers Fabr.* **2008**, *3* (1), 155892500800300.

(6) Asakura, T.; Ashida, J.; Yamane, T.; Kameda, T.; Nakazawa, Y.; Ohgo, K.; Komatsu, K. A repeated β-turn structure in poly (Ala-Gly) as a model for silk I of Bombyx mori silk fibroin studied with two-dimensional spin-diffusion NMR under off magic angle spinning and rotational echo double resonance. *J. Mol. Biol.* **2001**, *306* (2), 291−305.

(7) Wnek, G. E.; Bowlin, G. L. *Encyclopedia of Biomaterials and Biomedical Engineering*; CRC Press, 2008.

(8) Riley, S. L.; Dutt, S.; De La Torre, R.; Chen, A. C.; Sah, R. L.; Ratcliffe, A. Formulation of PEG-based hydrogels affects tissue-engineered cartilage construct characteristics. *J. Mater. Sci.: Mater. Med.* **2001**, *12* (10−12), 983−990.

(9) Huang, Z.-M.; Zhang, Y.-Z.; Kotaki, M.; Ramakrishna, S. A review on polymer nanofibers by electrospinning and their applications in nanocomposites. *Compos. Sci. Technol.* **2003**, *63* (15), 2223−2253.

(10) Matthews, J. A.; Boland, E. D.; Wnek, G. E.; Simpson, D. G.; Bowlin, G. L. Electrospinning of collagen type II: a feasibility study. *J. Bioact. Compat. Polym.* **2003**, *18* (2), 125−134.

(11) Boland, E. D.; Coleman, B. D.; Barnes, C. P.; Simpson, D. G.; Wnek, G. E.; Bowlin, G. L. Electrospinning polydioxanone for biomedical applications. *Acta Biomater.* **2005**, *1* (1), 115−123.

(12) Stankevich, K. S.; Kudryavtseva, V. L.; Bolbasov, E. N.; Shesterikov, E. V.; Larionova, I. V.; Shapovalova, Y. G.; Domracheva, L. V.; Volokhova, A. A.; Kurzina, I. A.; Zhukov, Y. M.; Malashicheva, A. B.; Kzhyshkowska, J. G.; Tverdokhlebov, S. I. Modification of PCL scaffolds by reactive magnetron sputtering: a possibility for modulating macrophage responses. *ACS Biomater. Sci. Eng.* **2020**, *6*, 3967.

(13) Mooney, D. J.; Langer, R. S. Engineering biomaterials for tissue engineering: The 10−100 micron size scale. *Tissue Engineering*; CRC Press, **2003**; Vol *12*, p 11-1,.

(14) Rosso, F.; Marino, G.; Giordano, A.; Barbarisi, M.; Parmeggiani, D.; Barbarisi, A. Smart materials as scaffolds for tissue engineering. *J. Cell. Physiol.* **2005**, *203* (3), 465−470.

(15) Altman, G. H.; Diaz, F.; Jakuba, C.; Calabro, T.; Horan, R. L.; Chen, J.; Lu, H.; Richmond, J.; Kaplan, D. L. Silk-based biomaterials. *Biomaterials* **2003**, *24* (3), 401−416.
(16) Gomes, M.; Azevedo, H.; Malafaya, P.; Silva, S.; Oliveira, J.; Silva, G.; Sousa, R.; Mano, J.; Reis, R. Natural polymers in tissue engineering applications. In *Tissue Engineering*; Elsevier, 2008; pp 145−192.
(17) Baker, S. R.; Banerjee, S.; Bonin, K.; Guthold, M. Determining the mechanical properties of electrospun poly-ε-caprolactone (PCL) nanofibers using AFM and a novel fiber anchoring technique. *Mater. Sci. Eng., C* **2016**, *59*, 203−212.
(18) Brown, T. D.; Dalton, P. D.; Hutmacher, D. W. Direct writing by way of melt electrospinning. *Adv. Mater.* **2011**, *23* (47), 5651−5657.
(19) Engel, E.; Michiardi, A.; Navarro, M.; Lacroix, D.; Planell, J. A. Nanotechnology in regenerative medicine: the materials side. *Trends Biotechnol.* **2008**, *26* (1), 39−47.
(20) Falconnet, D.; Csucs, G.; Grandin, H. M.; Textor, M. Surface engineering approaches to micropattern surfaces for cell-based assays. *Biomaterials* **2006**, *27* (16), 3044−3063.
(21) Ishaug-Riley, S. L.; Okun, L. E.; Prado, G.; Applegate, M. A.; Ratcliffe, A. Human articular chondrocyte adhesion and proliferation on synthetic biodegradable polymer films. *Biomaterials* **1999**, *20* (23−24), 2245−2256.
(22) Long, J.; Etxeberria, A. E.; Nand, A. V.; Bunt, C. R.; Ray, S.; Seyfoddin, A. A 3D printed chitosan-pectin hydrogel wound dressing for lidocaine hydrochloride delivery. *Mater. Sci. Eng., C* **2019**, *104*, 109873.
(23) Ahmed, J.; Mulla, M.; Maniruzzaman, M. Rheological and Dielectric Behavior of 3D-Printable Chitosan/Graphene Oxide Hydrogels. *ACS Biomater. Sci. Eng.* **2020**, *6* (1), 88−99.
(24) Chen, G.; Sun, Y.; Lu, F.; Jiang, A.; Subedi, D.; Kong, P.; Wang, X.; Yu, T.; Chi, H.; Song, C.; Liu, K.; Qi, P.; Yan, J.; Ji, Y. A three-dimensional (3D) printed biomimetic hierarchical scaffold with a covalent modular release system for osteogenesis. *Mater. Sci. Eng., C* **2019**, *104*, 109842.
(25) Serra, T.; Planell, J. A.; Navarro, M. High-resolution PLA-based composite scaffolds via 3-D printing technology. *Acta Biomater.* **2013**, *9* (3), 5521−5530.
(26) Koroleva, A.; Gill, A.; Ortega, I.; Haycock, J.; Schlie, S.; Gittard, S.; Chichkov, B.; Claeyssens, F. Two-photon polymerization-generated and micromolding-replicated 3D scaffolds for peripheral neural tissue engineering applications. *Biofabrication* **2012**, *4* (2), 025005.
(27) Weiß, T.; Hildebrand, G.; Schade, R.; Liefeith, K. Two-photon polymerization for microfabrication of three-dimensional scaffolds for tissue engineering application. *Eng. Life Sci.* **2009**, *9* (5), 384−390.
(28) Serien, D.; Sugioka, K. Three-Dimensional Printing of Pure Proteinaceous Microstructures by Femtosecond Laser Multiphoton Cross-Linking. *ACS Biomater. Sci. Eng.* **2020**, *6* (2), 1279−1287.
(29) Claeyssens, F.; Hasan, E. A.; Gaidukeviciute, A.; Achilleos, D. S.; Ranella, A.; Reinhardt, C.; Ovsianikov, A.; Shizhou, X.; Fotakis, C.; Vamvakaki, M.; Chichkov, B. N.; Farsari, M. Three-dimensional biodegradable structures fabricated by two-photon polymerization. *Langmuir* **2009**, *25* (5), 3219−3223.
(30) de Amorim Almeida, H.; da Silva Bártolo, P. J. Virtual topological optimization of scaffolds for rapid prototyping. *Medical Engineering Physics* **2010**, *32* (7), 775−782.
(31) Yang, Y.; Basu, S.; Tomasko, D. L.; Lee, L. J.; Yang, S.-T. Fabrication of well-defined PLGA scaffolds using novel micro-embossing and carbon dioxide bonding. *Biomaterials* **2005**, *26* (15), 2585−2594.
(32) Yu, Y.; Addai-Mensah, J.; Losic, D. Synthesis of self-supporting gold microstructures with three-dimensional morphologies by direct replication of diatom templates. *Langmuir* **2010**, *26* (17), 14068−14072.
(33) Gallego, D.; Ferrell, N.; Sun, Y.; Hansford, D. J. Multilayer micromolding of degradable polymer tissue engineering scaffolds. *Mater. Sci. Eng., C* **2008**, *28* (3), 353−358.
(34) Ermis, M.; Antmen, E.; Hasirci, V. Micro and Nanofabrication methods to control cell-substrate interactions and cell behavior: A review from the tissue engineering perspective. *Bioactive materials* **2018**, *3* (3), 355−369.
(35) Martella, D.; Parmeggiani, C. Advances in cell scaffolds for tissue engineering: the value of liquid crystalline elastomers. *Chem. - Eur. J.* **2018**, *24* (47), 12206−12220.
(36) Abgrall, P.; Conedera, V.; Camon, H.; Gue, A. M.; Nguyen, N. T. SU-8 as a structural material for labs-on-chips and micro-electromechanical systems. *Electrophoresis* **2007**, *28* (24), 4539−4551.
(37) Lowery, J. L.; Datta, N.; Rutledge, G. C. Effect of fiber diameter, pore size and seeding method on growth of human dermal fibroblasts in electrospun poly (ε-caprolactone) fibrous mats. *Biomaterials* **2010**, *31* (3), 491−504.
(38) Venugopal, J.; Ma, L.; Yong, T.; Ramakrishna, S. In vitro study of smooth muscle cells on polycaprolactone and collagen nanofibrous matrices. *Cell Biol. Int.* **2005**, *29* (10), 861−867.
(39) Liu, J.; Shen, X.; Tang, S.; Li, H.; Mei, S.; Zheng, H.; Sun, Y.; Zhao, J.; Kaewmanee, R.; Yang, L.; Gan, Q.; Wei, J. Improvement of rBMSCs Responses to Poly (propylene carbonate) Based Biomaterial through Incorporation of Nanolaponite and Surface Treatment Using Sodium Hydroxide. *ACS Biomater. Sci. Eng.* **2020**, *6* (1), 329−339.

https://doi.org/10.1021/acsbiomaterials.1c00651
ACS Biomater. Sci. Eng. 2021, 7, 4763−4778